An Analysis of Respiratory Rhythm in Normal Subjects Using Nonlinear Dynamics

非線形システム論による正常成人の呼吸リズムの解析

赤木　美智男

①

An Analysis of Respiratory Rhythm in Normal Subjects Using Nonlinear Dynamics

非線形システム論による
正常成人の呼吸リズムの解析

赤木 美智男

An analysis of respiratory rhythm in normal subjects using nonlinear dynamics

Michio Akagi

KEY WORDS

Regulation of respiration, breath-to-breath fluctuation of respiratory parameters, human, nonlinear dynamics, chaos

ABSTRACT

In order to investigate whether the breath-to-breath fluctuation of respiratory parameters are due to deterministic dynamics (chaos or quasiperiodicity) of the respiratory controlling system, respiratory patterns were recorded by the respiratory inductive plethysmograph in six healthy adults during sleep, and analyzed using the algorithms of nonlinear dynamics. Analytic methods including the plotting of return maps, the calculation of the correlation dimension and the maximal Lyapunov exponent, the nonlinear prediction method, and the average directional vector method were employed to detect deterministic dynamics in the tidal volume curves obtained from the subjects. We could not find any clear evidence of determinism using any of these methods, and thus conclude that the variability of respiratory parameters during sleep was due to random fluctuations or high-dimensional determinism of the respiratory controlling system and not chaos.

I. INTRODUCTION

The existence of breath-to-breath fluctuations of respiration has been known for decades. Whether these apparently random fluctuations are due to deterministic dynamics or just random noise has been investigated using various analytic methods, including spectral analysis, an autoregression model, comb filtering, and turning point analysis.[1-11] These studies have revealed that the breath-to-breath variability of respiratory parameters is not the result of a completely random process but of a deterministic one. However, the methods used in the studies could not fully explain the dynamics, or needed to assume the existence of a stochastic process in the respiratory controlling system to explain its nonperiodic behavior.

Recently, methods of nonlinear dynamics, or chaos theory, have been applied to various biological systems[12] which show complex rhythmicity such as the nervous system and the circulatory system. The respiratory system has also been studied using this approach[13-18], but there are relatively few studies focused on normal respiratory rhythm. Sammon and Bruce[19] analyzed respiration in rats, and concluded that it was chaotic. Donaldson[20] argued that respiration of resting humans was chaotic. On the other hand, DeGoede *et al.*[21] studied respiration in cats, and found no evidence of chaos. Thus, definitive conclusions have not been reached concerning the dynamics which cause breath-to-breath fluctuations of respiration.

The aim of this study was to use analytic methods of nonlinear dynamics to investigate whether breath-to-breath fluctuations of respiratory parameters result from the deterministic dynamics of the respiratory controlling system. If so, it is feasible to express behaviour of the controlling system in nonlinear differential equations, although more knowledge about the structure and the function of the system is necessary. Then, the mechanism of pathological respiratory rhythm such as apnea attack and Chayne-Stokes breathing can be understood more in detail, and sudden change of respiratory patterns may become predictable by measuring proper parameters. On the other hand, if breath-to-breath fluctuations are due to random process, respiration is understood to be controlled fuzzily. Methods of analyzing such systems, or a mixture of determinism and a random process, are

not fully established. The results of our study indicate that human respiration during sleep does not appear to be chaotic.

II. METHODS

Changes in lung volume were continuously measured in six healthy adults during sleep using a respiratory inductive plethysmograph (RIP). Proper data sets of each sleep stage were chosen from the whole recording and analyzed using the analytic methods described below. Since there is no uniformly accepted method of definitively assessing the presence or absence of chaos in complicated systems, a number of standard algorithms of nonlinear dynamics were employed, including the plotting of return maps, the calculation of the fractal dimension of the attractor[22,23] and the maximal Lyapunov exponent[24], the nonlinear prediction method proposed by Sugihara and May[25], and the method of average directional vectors proposed by Kaplan and Glass[26,27]. To assess the results of the calculations, simulation data were created and compared with the experimental data.

A. Subjects

Six healthy, non-smoking adults were examined. Properties of the subjects are summarized in Table 1. They had no symptoms or signs of respiratory diseases, or of sleep disorders. To minimize the influences of external or internal (psychological) perturbation, data were taken while the subjects were asleep. The experiments were performed at night so as to simulate a natural sleep environment.

Table 1. Subjects and data sets

Subject	Age	Sex	Race	Height	Weight	Sleep Stage	Data Length (minutes)	Number of breaths
#1	42	M	Oriental	165	63	II	11.0	144
						II	24.5	263
						SW†	19.5	262
						SW	13.5	164
						REM‡	8.5	110
#2	30	M	Oriental	168	59	I	11.0	181
						II	19.0	264
						SW	23.5	340
						SW	15.0	221
						REM	9.5	158
#3	31	M	Caucasian	173	77	II	20.5	332
						II	20.0	304
						SW	11.0	191
						REM	15.5	266
						REM	10.5	179
#4	24	M	Oriental	172	85	II	16.5	217
						II	13.5	188
						SW	20.5	283
						REM	14.0	193
						REM	11.0	143
#5	32	F	Caucasian	158	56	II	11.5	185
						II	15.0	230
						SW	8.5	130
						REM	9.5	169
#6	27	M	Caucasian	173	68	II	18.0	231
						II	16.0	202
						SW	10.0	133
						REM	36.5	498

† slow wave sleep, ‡ rapid eye movement sleep

B. Respiratory inductive plethysmograph (RIP)

A respiratory inductive plethysmograph (Respitrace™, Ambulatory Monitoring Inc., New York) was used to measure changes in lung volume to avoid the effect on breathing pattern introduced by use of a mouthpiece or noseclips[28,29,30]. The RIP is a device that measures movements of the thorax and abdomen. It consists of two elastic bands (transducers) with a coil of wire enmeshed, which are placed around the rib cage and abdomen. Changes in the cross-sectional area of rib cage and abdominal compartments, resulting from respiration, cause proportional changes in the inductance of the coils. Measurement of ventilation using the RIP is based upon the assumption that changes of lung volume can be approximated with two degrees of freedom of motion, *i.e.* rib cage and abdominal compartmental excursion. It is known to be quite accurate if properly calibrated[31].

To calibrate the RIP, the isovolume maneuver[32] was utilized to determine the ratio of the signals from the rib cage band to the abdominal band. Then, we recorded data while the subject took a few breaths from a 800 ml plastic bag. These data were used to convert voltage to volume measurement.

C. Experimental settings

The experiments were performed in the sleep laboratory, St. Michael Hospital, Toronto, which has two small units with a bed and measuring devices. Thus, two subjects were examined on the same day. Signals from the RIP were digitized using a 12 bit analog-digital converter with a sampling frequency of 100 Hz, and the digitized data were stored in a personal computer system. The electroencephalogram and the electroocurogram were also recorded to identify sleep stages as determined using the system of Rechtschaffen and Kales[33]. Data were recorded until the subjects had completed all stages of sleep.

D. Data processing

The sections of the RIP data which satisfied the following three criteria were selected for analysis (table 1):

(1) The sections could not contain data from different sleep stages.

(2) A sleep stage had to last for approximately ten minutes or more.

(3) The sections could not contain data where postural change occurred.

Since the RIP output signals were not contaminated with high-frequency noise, a low-pass filter was not utilized at the time of data acquisition. To smooth out the quantization effect caused by analog-digital conversion, a polynomial smoothing digital filter (Savitzky-Golay[34]) was applied, which is almost equivalent to using a low-pass filter of cut-off frequency of 4 Hz when the sampling frequency is 100 Hz and the window width is 21 points. Instantaneous flow was calculated as the first differential of the volume at the time of digital filtering to identify the phase of each breath. The beginning of each inspiratory and expiratory phase was determined by noting the point at which the sign of the flow signal changed.

E. Data analysis

1. Embedding

Since we assumed that our analyzed data sets were obtained in steady states, the variables of the system were assumed to move along the trajectory on the attractor. To reconstruct the attractor in a phase space from the one variable measured during the experiments, *i.e.* lung volume, the technique of embedding (Takens[35]) was employed. That is to say, an m-dimensional vector set $\{\boldsymbol{x}_i\}$ was produced from a scalar time series $\{x_i\}$ using time delay coordinates:

$$\boldsymbol{x}_i = (x_i, x_{i+\tau}, x_{i+2\tau}, \cdots, x_{i+(m-1)\tau})^t, \tag{1}$$

where $()^t$ denotes the transposed vector. The delay time τ was chosen as the first zero crossing of the autocorrelation function[36].

2. Return maps

Return maps of respiratory parameters of each breath were plotted to estimate low dimensional determinism. Inspiratory time, expiratory time, total respiratory time, and tidal

volume of each breath (T_{i_k}, T_{e_k}, T_{t_k}, and V_{t_k} respectively) were plotted against those of the following breath ($T_{i_{k+1}}$, $T_{e_{k+1}}$, $T_{t_{k+1}}$, and $V_{t_{k+1}}$). This procedure is equivalent to plotting Poincaré maps from the section where $dVolume/dt = 0$.

3. Correlation dimension

To calculate the fractal dimension of the attractor, the Grassberger-Procaccia algorithm[22,23] was chosen.

For the points $\{\boldsymbol{x}_n\} = \{\boldsymbol{x}_1, \boldsymbol{x}_2, \ldots, \boldsymbol{x}_n\}$ on the attractor embedded in a phase space, the correlation integral

$$C(r) = \frac{1}{ns} \sum_{i=1}^{s} \sum_{j=1}^{n} \Theta(r - \|\boldsymbol{x}_i - \boldsymbol{x}_j\|) \tag{2}$$

was estimated, where n is the number of the points on the attractor, s is the number of randomly sampled points, $\| \ \|$ denotes the norm of a vector (the Euclidean norm was employed in this study), and Θ is the Heaviside function. The purpose of using s as opposed to n was to reduce the calculation time. The correlation dimension D_c was defined as follows;

$$D_c = \lim_{r \to 0} \lim_{n,s \to \infty} \frac{\ln[C(r)]}{\ln r}. \tag{3}$$

For practical purposes, a proper interval of r where there is linear relationship between $\ln[C(r)]$ and $\ln r$ was chosen. To avoid obtaining spurious estimates of the dimension by oversampling and counting pairs of points which were too close in time[36,37], one in every ten points was used in the calculations, and Theiler's[38] modified algorithm was applied as well. Thus, the total number of points n used in the calculations varied between 6000 and 20000. The number of randomly sampled points s was 1000.

4. Lyapunov exponent

The maximal Lyapunov exponent was calculated as follows using the algorithm (fixed evolution time program) proposed by Wolf, Swift, Swinney, and Vastano[24] (WSSV algorithm).

Let a vector time series $\{\boldsymbol{x}_n\} = \{\boldsymbol{x}_1, \boldsymbol{x}_2, ..., \boldsymbol{x}_n\}$ be the points on the attractor embedded in a proper-dimensional phase space. First, the nearest neighbor to the initial point is located, and the distance (Euclidean norm) between these points is denoted by $L(t_0)$. At a later time t_1, the initial length $L(t_0)$ will have evolved to length $L'(t_1)$. The Lyapunov exponent is defined as the expanding (or shrinking) rate of $L'(t_1)/L(t_0)$, but the evolution time Δt ($= t_1 - t_0$) should be short enough so that only the small scale structure of the attractor is examined. Therefore, to examine the expanding rate of nearby trajectories through the attractor, a new point is searched for every Δt. Two criteria that the new point has to satisfy reasonably well are that its distance from the evolved fiducial point is small, and that the angular separation between the evolved and replacement elements is small. It is sometimes impossible to fulfill both criteria at the same time because the number of points in the data set is limited. To choose each point so that it best meets the two criteria, a modified algorithm proposed by Frank *et al.*[39] was employed, *i.e.* a weight function

$$w(r,\theta) = \left[a + \beta\left(\frac{b-r}{b-a}\right)^{\gamma} \right] \cos\theta \qquad (4)$$

was used, where b is the maximal length cutoff, a is the minimal length cutoff (usually set to the noise level), r denotes the distance between the candidate and the evolved fiducial point, θ denotes the angular separation between the evolved displacement vector and the candidate replacement vector, and α, β, and γ are numeric parameters, which were set to 0.1, 0.9, and 3 respectively. This procedure is repeated until the fiducial trajectory has traversed the entire data set. Lastly, the maximal Lyapunov exponent λ_1 is estimated as follows;

$$\lambda_1 = \frac{1}{t_M - t_0} \sum_{k=1}^{M} \log_2 \frac{L'(t_k)}{L(t_{k-1})} \quad (\text{bits / sec}), \qquad (5)$$

where M is the total number of replacement steps. Such parameters as the embedding dimension, the evolution time† , and the maximal and minimal length cutoffs have to be chosen carefully, but unfortunately there is no *a priori* way of giving them the appropriate values. Therefore, several almost arbitrarily chosen values were tried in the calculations.

5. Nonlinear prediction method

Several algorithms of this method have been proposed[25,42-45]. The algorithm of Sugihara and May[25] was employed in this study.

A time series $\{x_n\} = \{x_1, x_2, ..., x_n\}$ is first embedded in an m-dimensional phase space using time delay coordinates

$$\boldsymbol{x}_i = (x_i, x_{i-\tau}, ..., x_{i-(m-1)\tau})^t, \tag{6}$$

where τ is the delay time, and $()^t$ denotes the transposed vector (note the difference of the sign compared to Eq. 1). Then the vector time series $\{\boldsymbol{x}_n\}$ is separated in the middle, the first half being used as a database, and the second for prediction. Predictions are made using a simplex projection method. For a point $\boldsymbol{x}_i$ in the latter half, m+1 closest points are chosen from the former half. A prediction is obtained by following the trajectories of these nearby points and taking their weighted mean according to their original distance to $\boldsymbol{x}_i$. The accuracy of the predictions is assessed by using the correlation coefficient between observed and predicted values. In the case of chaotic data, prediction accuracy is high for a short

---

† According to Wolf *et al.*[24], the estimated λ_1 is fairly stable when the evolution time lies between about 20% to 140% of the mean orbital period for the Rössler attractor[40]. This does not necessarily hold true for other attractors. The modified algorithm of Frank *et al.*[39] includes a method to determine the proper evolution time as well as the new replacement technique mentioned in the body above, but it was not adopted, because our test of the algorithm using the Lorenz[41] attractor gave different results from what they showed in their paper.

prediction time because of its determinism, but accuracy decreases with each increment of prediction time due to its sensitive dependence on the initial conditions.

6. Kaplan-Glass algorithm[26, 27] using average directional vectors

Let a set of vectors $\{\boldsymbol{x}_n\}$ be the points on the trajectory embedded in an m-dimensional phase space. The phase space is coarse grained into a g^m grid, where $g \approx$ 4-32 depending on the data size, the embedding dimension, and the memory size and calculation time of the computer. Each pass k of the trajectory through a box j generates a vector of unit length called the trajectory vector $\boldsymbol{v}_{k,j}$, whose direction is the average direction of that pass of the trajectory in the box j. The set of average directional vectors in the box j are summarized as the resultant vector

$$\boldsymbol{V}_j = \sum_k \boldsymbol{v}_{k,j} / n_j , \tag{7}$$

where n_j is the number of passes through the box j. For the attractor of a deterministic system embedded in a proper-dimensional phase space, the length of each resultant vector $|\boldsymbol{V}_j|$ is almost 1 because the average directional vectors are well aligned. Thus, whether the system is deterministic or not can be tested by observing the mean value of $|\boldsymbol{V}_j|$ for all the boxes:

$$\overline{L}_n^m = \left\langle |\boldsymbol{V}_j| \right\rangle_{j \text{ such that the number of passes} = n} , \tag{8}$$

where $\langle\ \rangle$ denotes the arithmetic mean. In some cases it is convenient to combine the $\overline{L}_n^m$ for a given embedding into a single number $\overline{\Lambda}$ and to plot $\overline{\Lambda}$ against the delay time τ, because $\overline{L}_n^m$ is sensitive to τ. $\overline{\Lambda}$ is defined as the weighted average of $\overline{L}_n^m$, *i.e.*

$$\overline{\Lambda} = \frac{1}{\sum_j n_j} \sum_j n_j \frac{(\overline{L}_{n_j}^m)^2 - (\overline{R}_{n_j}^m)^2}{1 - (\overline{R}_{n_j}^m)^2} , \tag{9}$$

where $\overline{R}_n^m$ is $\overline{L}_n^m$ for a random walk, *i.e.*

$$\overline{R}_n^m = \left(\frac{2}{m}\right)^{1/2} \frac{\Gamma[(m+1)/2]}{\Gamma(m/2)} n^{-1/2}, \tag{10}$$

where Γ is the gamma function. For completely random processes such as a random walk and Gaussian noise, $\overline{\Lambda}$ is always 0 regardless of τ. On the other hand, for purely

deterministic dynamics, $\overline{\Lambda}$ is always 1. Determinism of a system is tested by comparing its $\overline{\Lambda}$ with that of a random process, which is, in our study, consisted of the simulated time series described below.

7. Simulation

In order to conclude that the experimental data are chaotic, it is essential to show a clear difference between the experimental data and the nonchaotic data employed as the null hypothesis, because analytic methods of nonlinear dynamics which can differentiate chaos from other dynamics may sometimes give similar results for both chaotic and nonchaotic data in practice[46]. In some previous studies, uncorrelated white noise or a limit cycle combined with uncorrelated white noise was employed as the null hypothesis. However, these nonchaotic models are not appropriate in our case, because the volume curves are so periodic and smooth that they are obviously different from white noise or a limit cycle contaminated with white noise. It may be useful to employ surrogate data generated by randomizing the phases of the Fourier transform of the original time series as the null hypothesis[27]. However, as shown in Fig. 1, one can easily tell the difference between the two by eye.

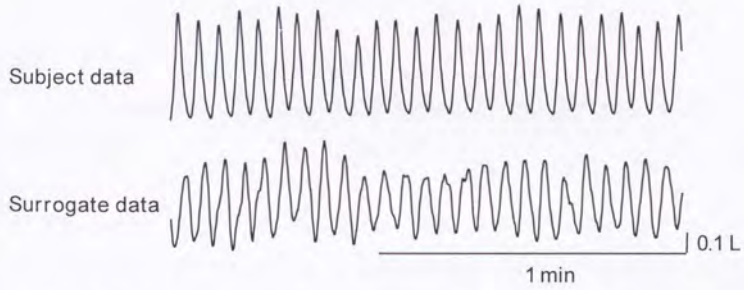

Fig. 1 Subject data and Surrogate data. The difference between the two is clear.

Hence, a simulated time series was created from the subject data as described in Fig. 2, so that the real data and the simulated data had the same periodicity, the same breath-to-breath variability (in a statistical sense), and a similar power spectrum. Since the breath-to-breath variations of the simulation were produced randomly, *i.e.* successive breaths had no relation in terms of phase or tidal volume to each other, the dynamics of the simulation is categorized as a "noisy limit cycle," but *not as chaos*. The time series, the reconstructed attractors in three-dimensional phase space, and the power spectra of the subject data and the simulated data are shown in Fig. 3.

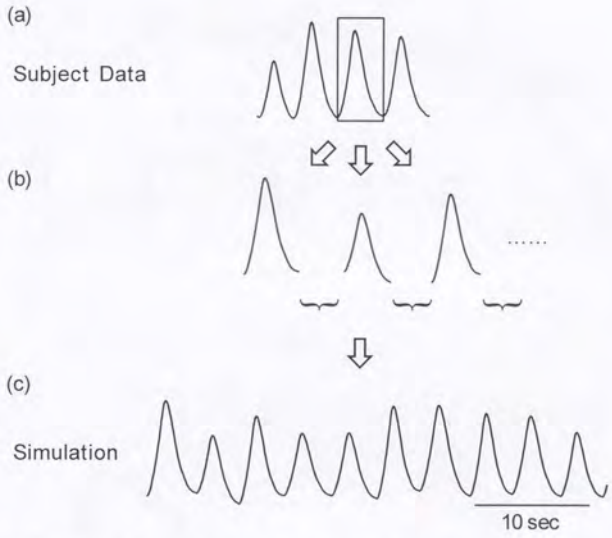

Fig. 2 Creation of a simulated time series. (a) Select a typical one breath pattern from the subject data. (b) Stretch or shorten this pattern along the time axis and the volume axis randomly, so that the mean and the standard deviation of total respiratory time, tidal volume, and the volume at the end of expiration (equivalent to the functional residual capacity) are the same as those of the subject data. (c) Connect each distorted breath wave.

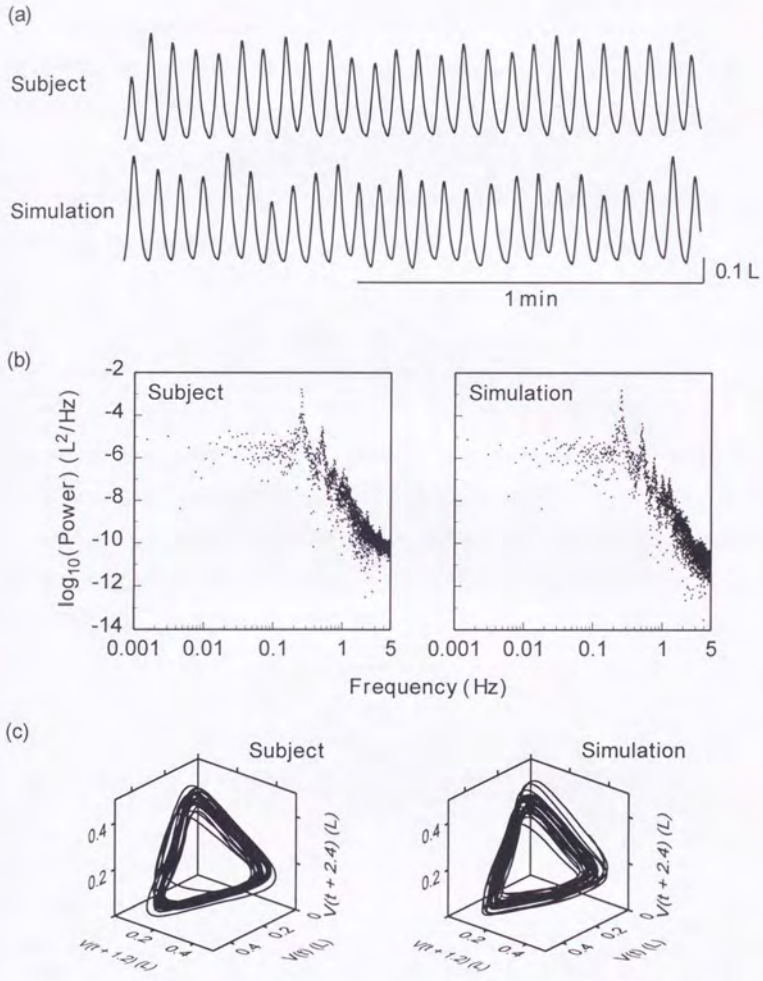

Fig. 3 (a) Time courses, (b) Power spectra, and (c) Reconstructed attractors in a three-dimensional phase space, of subject #5 (stage II sleep) and the simulation.

8. An example of chaos

To verify the computer programs of the analytic methods coded by the author, a mathematical model which is known to be chaotic was employed and analyzed prior to the experimental data. The Rössler model[40] was chosen for this purpose because its characteristics have been studied in detail.

The Rössler model consists of three coupled ordinary differential equations which contain only one nonlinear term:

$$\begin{aligned} dx/dt &= -(y+z) \\ dy/dt &= x+ay \\ dz/dt &= b+z(x-c) \end{aligned} \tag{10}$$

It shows periodic, quasiperiodic, and chaotic behaviour according to the values of the parameters a, b, and c, *e. g.* (a = 0.05, b = 0.2, c = 10), (a = 0.105, b = 0.2, c = 10), and (a = 0.15, b = 0.2, c = 10) respectively. The time courses of x, y, and z, and the attractor in three dimensional phase space for three different values of parameter a are shown in Fig. 4. The *chaotic* time series of variable x was analyzed and compared with the experimental data.

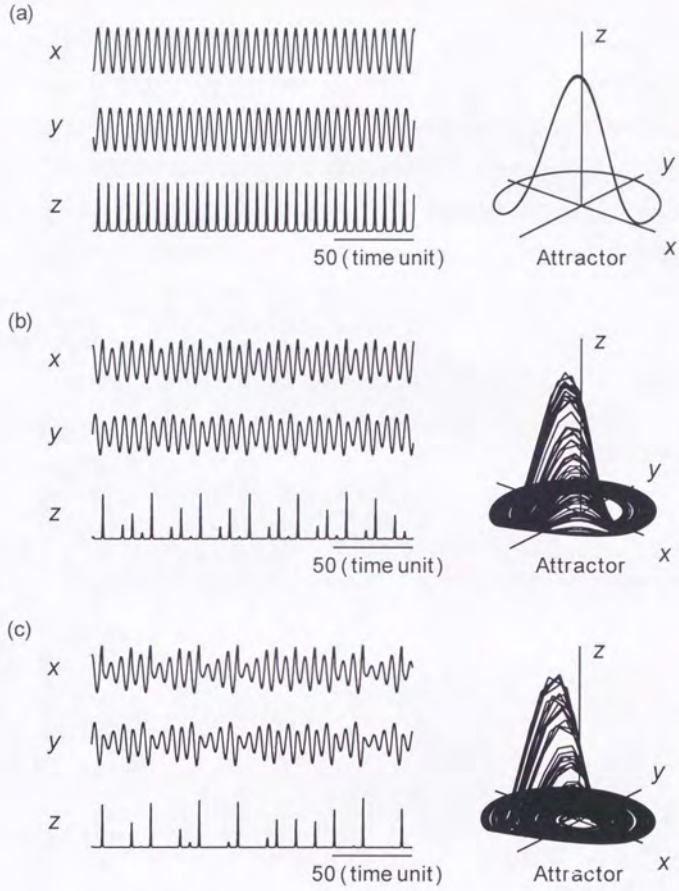

Fig. 4 Time courses of variable *x*, *y*, and *z* and attractors of the Rössler model for three different values of parameter *a*. The model is periodic (a), quasiperiodic (b), and chaotic (c) when parameter *a* equals 0.05, 0.105, and 0.15 respectively. In every case, parameter $b = 0.2$, and $c = 10$. It is not easy to differentiate (b) and (c) by eye.

III. RESULTS

Results from the Rössler model, subject #5, and the simulation are shown in this section. As the results from the other subjects were essentially the same as those from subject #5, they are not shown here except the results of the correlation dimension and Lyapunov exponent calculation, which are summarized in Table 2 (page 23). Subject #5 was chosen because the calibration procedure of the RIP was done most accurately, *i. e.* measurement noise was presumed to be the smallest in this subject.

A. Return maps

Return maps of the peak value (maxima) and the peak-to-peak time of the Rössler model are shown in Fig. 5. Those "V" or inverted "V" shaped maps indicate low-dimensional determinism.

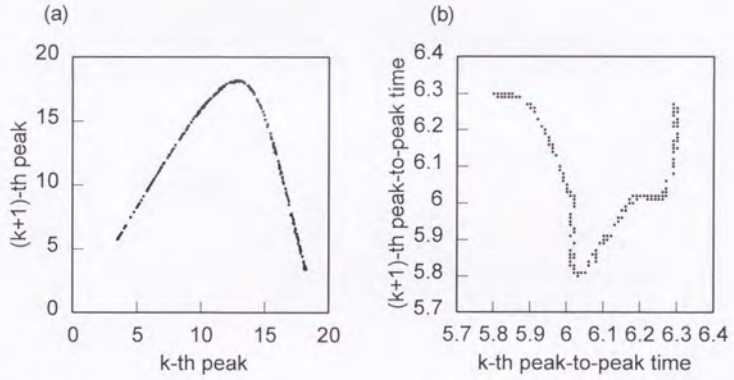

Fig. 5 Return maps of the Rössler model. (a) Map of the peak value of variable *x*, *i. e.* the relationship between the two successive peak values (maxima) of *x*. (b) Map of the peak-to-peak time of *x*.

Return maps of inspiratory time, expiratory time, total respiratory time, and tidal volume of subject #5 at stage II sleep, slow wave (SW) sleep, and rapid eye movement (REM) sleep are shown in Fig. 6, 7, and 8 respectively. The maps from both the subject data and the simulated data showed only a pattern of scattering points around the mean value instead of a special pattern suggesting determinism. This fact, however, does not necessarily mean that the subject data is not deterministic, because only low-dimensional (not much higher than two dimensional) dynamics can be detected by this method. Results from the other five subjects are not shown here because they were essentially the same as those from subject #5.

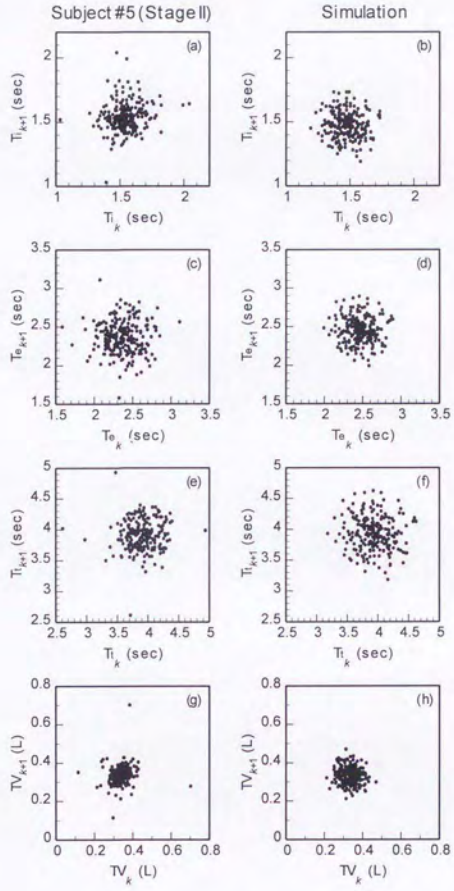

Fig. 6 Return maps of (a) and (b) Inspiration time, (c) and (d) Expiration time, (e) and (f) Total respiratory time, and (g) and (h) Tidal volume from subject #5 at stage II sleep and the simulation. Note that they do not reveal any special patterns such as a "V" shape or a more complicated shape, but merely a scattering of points around their mean values.

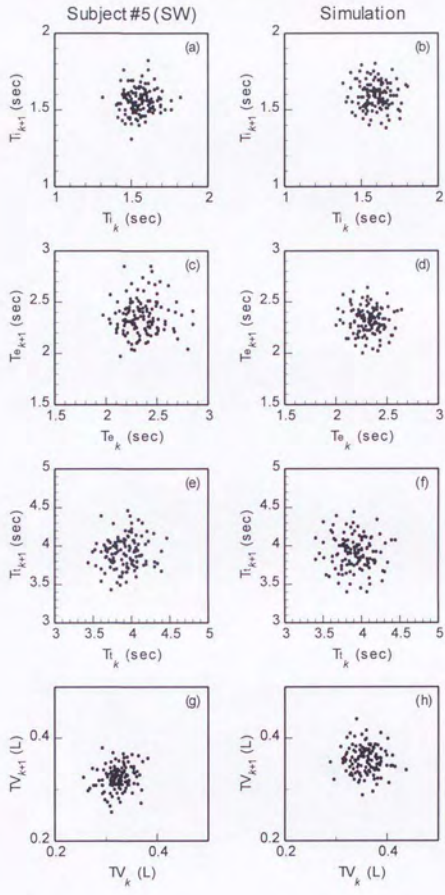

Fig. 7 Return maps of (a) and (b) Inspiration time, (c) and (d) Expiration time, (e) and (f) Total respiratory time, and (g) and (h) Tidal volume from subject #5 at SW sleep and the simulation.

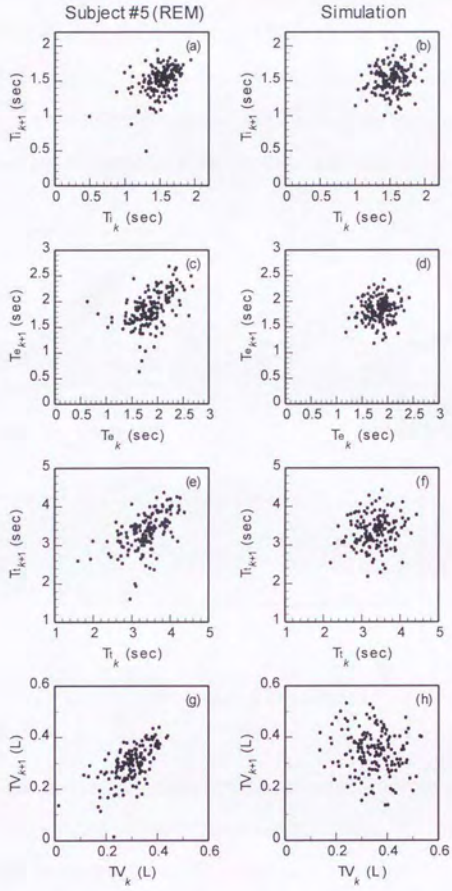

Fig. 8 Return maps of (a) and (b) Inspiration time, (c) and (d) Expiration time, (e) and (f) Total respiratory time, and (g) and (h) Tidal volume from subject #5 at REM sleep and the simulation.

B. The correlation dimension

The results of the calculation of the correlation dimension of the Rössler attractor are shown in Fig. 9. There was an interval of ln$r$ where the slope of ln[$C(r)$] was flat, or the scaling region. The slope in this region did not increase with the increment of the embedding dimension but approached a constant, *i. e.* the correlation dimension.

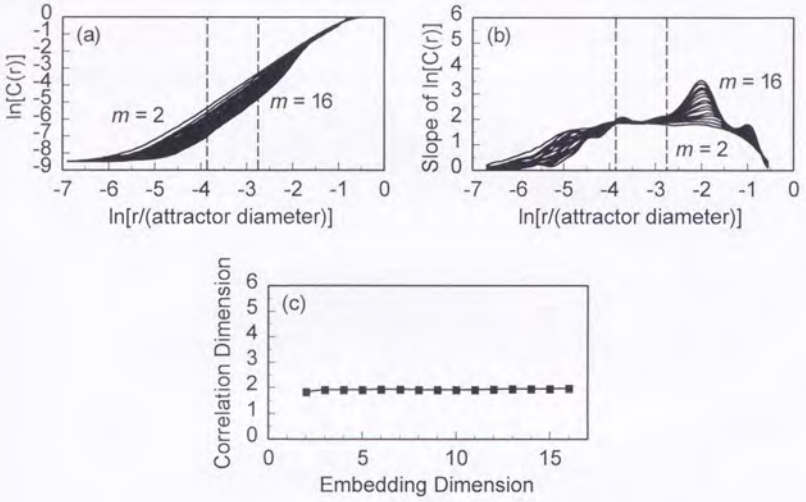

Fig. 9 Results of the calculation of the correlation dimension of the Rössler attractor. (a) ln[$C(r)$] *vs.* ln[r/(attractor diameter)], (b) Slope of ln[$C(r)$] *vs.* ln[r/(attractor diameter)], and (c) Estimated correlation dimension for each embedding dimension. $C(r)$ and m denote the correlation integral and the embedding dimension respectively, and the dotted lines show the scaling region. The total number of points n = 10000, the number of randomly sampled points s = 1000, and the delay time τ = 0.16 time unit.

The results from subject #5 at stage II sleep are illustrated in Fig. 10. Unlike the results from the chaotic data, neither the results from the subject data nor those from the simulated data had good scaling regions. Moreover, even though a correlation dimension was estimated for each embedding dimension by choosing a scaling region that appeared to be adequate, the estimated value continued to increase with each increment of the embedding dimension. Thus, the correlation dimension of the subject data as well as the simulated data could not be determined. These are characteristics of noisy dynamics, irrespective of the origin of the noise. The results from all the subjects are summarized in Table 2.

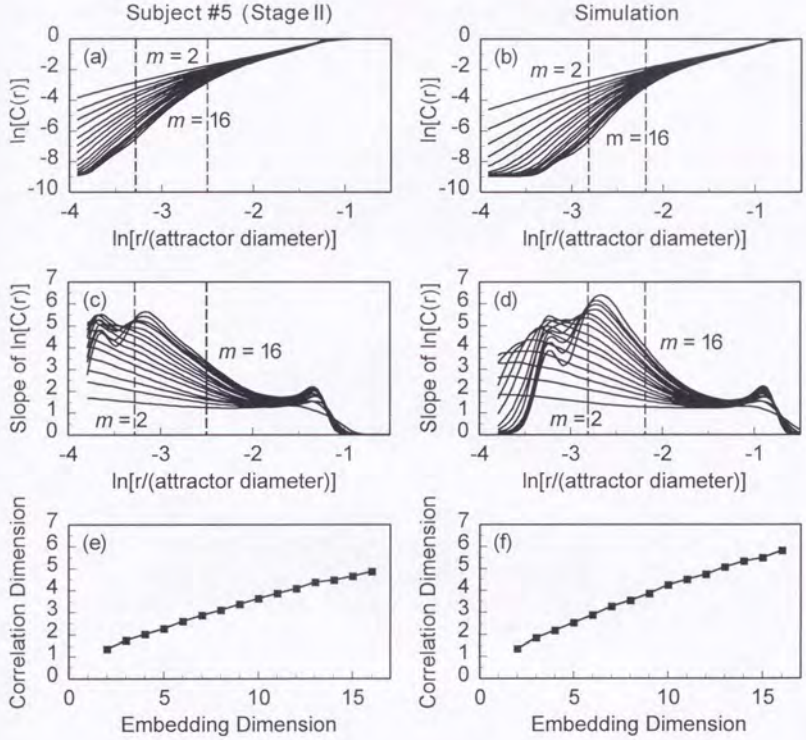

Fig. 10 Results of the calculation of the correlation dimension of the data from subject #5 at stage II sleep and the simulation. (a) and (b) ln[$C(r)$] *vs.* ln[r/(attractor diameter)], (c) and (d) Slope of ln[$C(r)$] *vs.* ln[r/(attractor diameter)], and (e) and (f) Estimated correlation dimension for each embedding dimension. The dotted lines show the almost arbitrarily chosen scaling region. The total number of points n = 8000, the number of randomly sampled points s = 1000, and the delay time τ = 1.2 sec.

Table 2. Summary of the results of the dimension and Lyapunov exponent calculation

Subject	Sleep Stage	Estimate of Dc†			Estimate of MLE‡ (bits/sec)		
		ED*=5	ED=10	ED=15	ED=3	ED=6	ED=9
#1	II	2.95	4.50	5.67	0.35	0.20	0.11
	II	2.68	4.13	5.38	0.47	0.27	0.18
	SW	2.60	4.00	4.95	0.47	0.26	0.18
	SW	2.55	3.98	4.94	0.44	0.25	0.15
	REM	2.46	3.77	4.72	0.39	0.25	0.17
#2	I	2.61	3.95	4.79	0.57	0.29	0.17
	II	2.81	4.13	5.17	0.53	0.25	0.08
	SW	2.36	3.96	5.14	0.55	0.32	0.21
	SW	2.26	3.69	4.90	0.56	0.31	0.23
	REM	2.36	3.78	4.83	0.54	0.31	0.21
#3	II	3.04	4.75	6.02	0.60	0.27	0.04
	II	2.75	4.26	5.39	0.58	0.26	0.07
	SW	2.84	4.57	5.77	0.58	0.28	0.19
	REM	2.83	4.26	5.11	0.58	0.30	0.19
	REM	2.74	4.24	5.31	0.55	0.27	0.18
#4	II	2.71	3.92	4.91	0.49	0.26	0.15
	II	2.64	3.82	4.49	0.43	0.29	0.16
	SW	2.73	4.41	5.79	0.49	0.27	0.18
	REM	2.70	3.93	4.99	0.45	0.27	0.18
	REM	2.79	4.29	5.33	0.44	0.25	0.18
#5	II	2.45	3.58	4.64	0.59	0.29	0.18
	II	2.31	3.78	4.91	0.44	0.27	0.19
	SW	2.59	3.93	4.70	0.54	0.28	0.16
	REM	2.25	3.54	4.56	0.62	0.31	0.18
#6	II	2.68	4.04	5.03	0.54	0.29	0.18
	II	2.27	3.68	4.70	0.46	0.26	0.18
	SW	2.49	3.89	4.93	0.51	0.30	0.21
	REM	2.35	3.66	4.63	0.44	0.28	0.18

† Correlation dimension, ‡ Maximal Lyapunov exponent, *Embedding dimension
Those estimates of the Dc and the MLE do not seem to represent the true Dc and MLE of the attractors because of their dependency on the ED (see the text).

C. The maximal Lyapunov exponent

The positive value of the Lyapunov exponent indicates sensitive dependency on the initial condition; therefore, it is a direct indicator of chaos. However, one should be careful in interpreting the results of the calculations, because the estimated values may be sensitive to such parameters as the evolution time, the maximal length cutoff, and the embedding dimension. Fig. 11 shows the results of the Lyapunov exponent calculation of the Rössler attractor. The estimate of the maximal Lyapunov exponent was stable in a relatively wide range of those parameters, and its value was concordant with that in the literature[24].

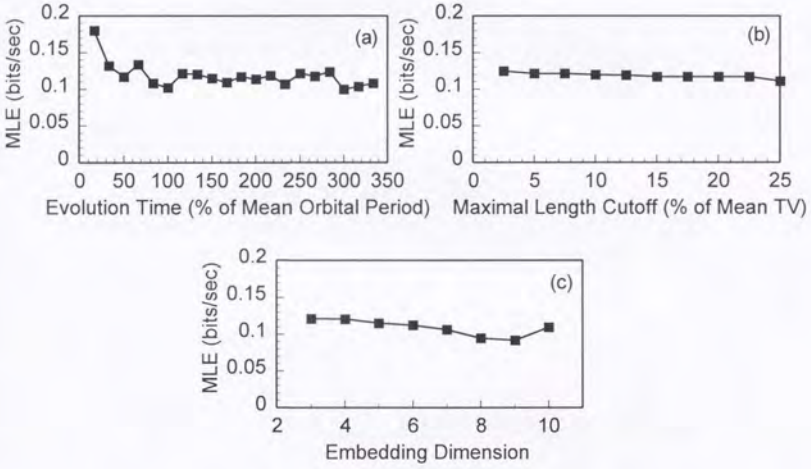

Fig. 11 Estimated maximal Lyapunov exponent (MLE) of the Rössler attractor for various parameters. (a) MLE *vs.* Evolution time. The embedding dimension (ED) is three, and the maximal length cutoff (MLC) is five percent of the attractor diameter. (b) MLE *vs.* MLC. The ED is three, and the evolution time is 150 percent of the mean orbital period. (c) MLE *vs.* ED. The MLC is five percent of the attractor diameter, and the evolution time is 150 percent of the mean orbital period.

On the other hand, the value obtained from both the subject data and the simulation was not stable when the evolution time or the embedding dimension was changed (Fig. 12). Furthermore, the estimate of the maximal Lyapunov exponent for the simulated data was positive. This estimate should not be positive because the dynamics of the simulation is not categorized as chaos but rather noisy periodicity. This shows that the algorithm is limited in its ability to detect chaos in this type of data set. Therefore, the positive Lyapunov exponent obtained from the subject data cannot be interpreted as evidence of chaos. Results of the calculation of the maximal Lyapunov exponent in all the subjects are summarized in Table 2 (page 23).

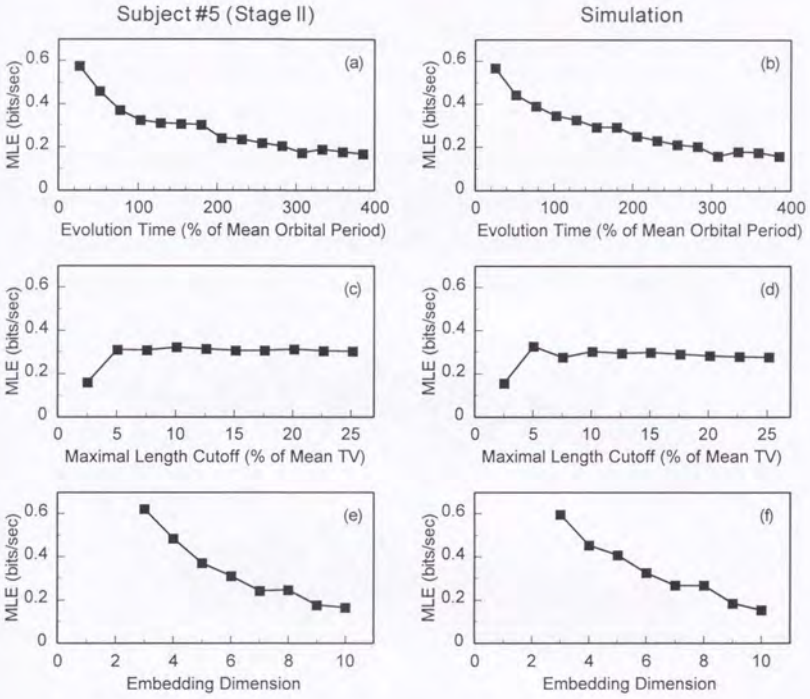

Fig. 12 Estimated MLE of the data from subject #5 and the simulation. (a) and (b) MLE *vs.* Evolution time. The ED is six, and the MLC is five percent of mean tidal volume (≈ the attractor diameter). (c) and (d) MLE *vs.* MLC. The ED is six, and the evolution time is 128 percent of the mean orbital period. (e) and (f) MLE *vs.* ED. The MLC is five percent of the mean tidal volume, and the evolution time is 128 percent of the mean orbital period. Note that the estimated MLE varies depending on the choice of these parameters, and that even the MLE of the simulated data, which should be zero theoretically, is estimated as a positive value by this algorithm.

D. Nonlinear prediction

Fig. 13 illustrates the results of the nonlinear prediction method from the Rössler model. Within the fifth peak value in the future, the correlation coefficient between the observed value and the predicted value was larger than 0.9. In other word, the prediction was accurate to the near future. However, the prediction accuracy suddenly declined with each increment of the prediction time. Those results reflected the characteristics of chaos, *i. e.* determinism and unpredictability due to sensitive dependence on initial conditions.

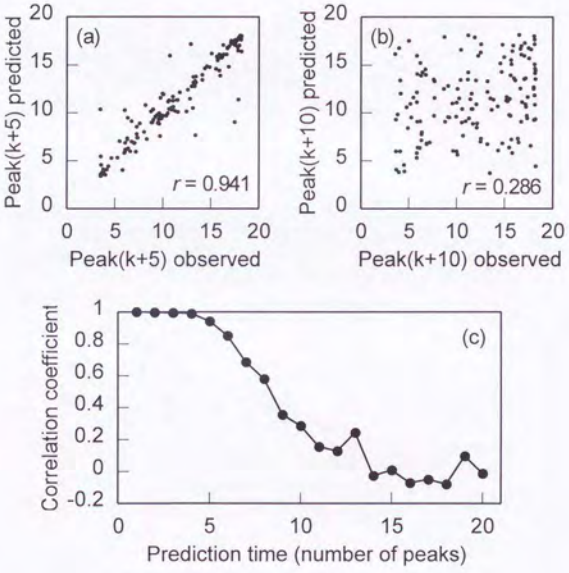

Fig. 13 Results of nonlinear prediction from the Rössler attractor. (a), (b) Correlation between the observed value and the predicted value of the fifth peak, and the tenth peak in the future respectively. (c) Prediction accuracy *vs.* prediction time. Prediction accuracy is high to the fifth peak value in the future, and then suddenly declines with the increment of prediction time.

The predictability of the subject data was accurate for a short period probably because of its high periodicity, but decreased gradually with each increment of prediction time (Fig. 14, 15, 16). However, these features do not necessarily indicate that the data derives from chaotic dynamics, because the results of the simulated data paralleled those of the subject data. Results from the other subjects, which are not shown here, were similar to those from subject #5.

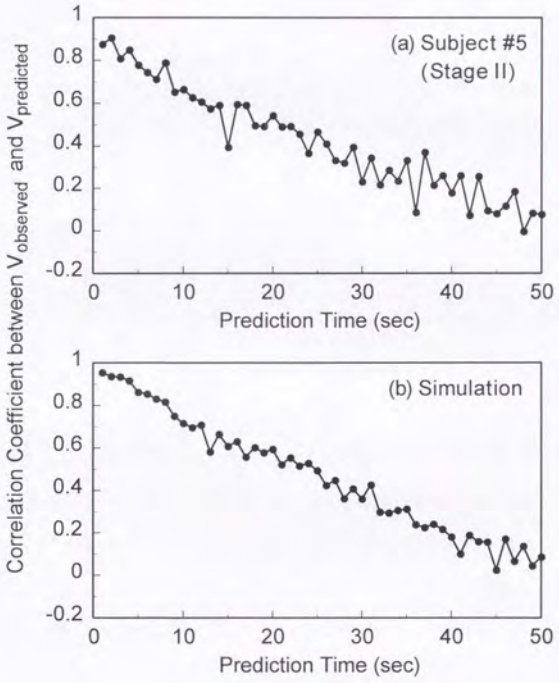

Fig. 14 Prediction accuracy *vs.* Prediction time calculated by the Sugihara-May algorithm. (a) Subject #5 (at stage II sleep), and (b) Simulation. The embedding dimension is six.

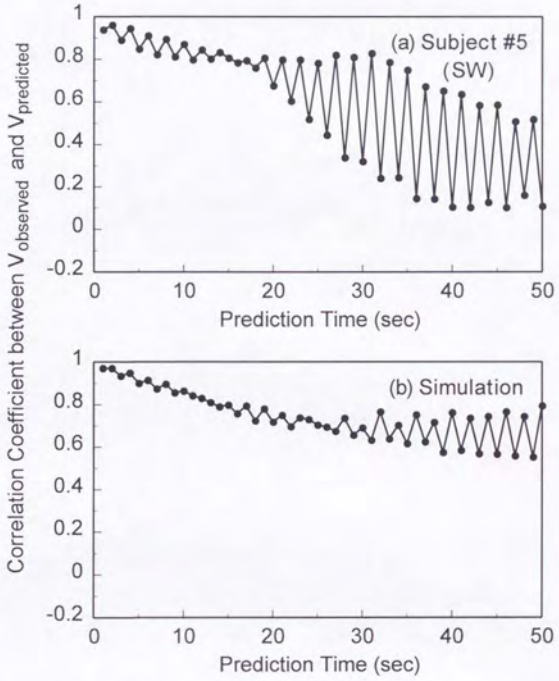

Fig. 15 Prediction accuracy *vs.* Prediction time. (a) Subject #5 (at SW sleep), and (b) Simulation. The embedding dimension is six. Prediction accuracy oscillates probably because respiration at SW sleep is almost periodic.

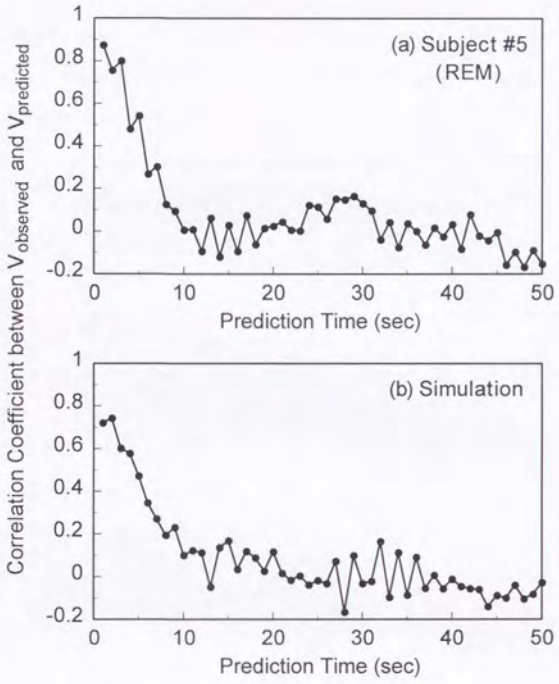

Fig. 16 Prediction accuracy *vs.* Prediction time. (a) Subject #5 (at REM sleep), and (b) Simulation. The embedding dimension is six. Prediction accuracy declines faster than that of stage II sleep and SW sleep probably because fluctuations of respiration at REM sleep are larger than those at the other stages. However, no significant difference is detected between the results of the subject data and the simulation.

E. Kaplan-Glass algorithm

Fig. 17 shows the function $\overline{\Lambda}(\tau)$, which denotes the weighted mean of the average directional vector of all the hyper cubes in the phase space, of the Rössler attractor and the surrogate data created from the Rössler attractor. $\overline{\Lambda}(\tau)$ of the Rössler attractor was significantly larger than that of the surrogate data, which means that the Rössler attractor is more deterministic than the surrogate data.

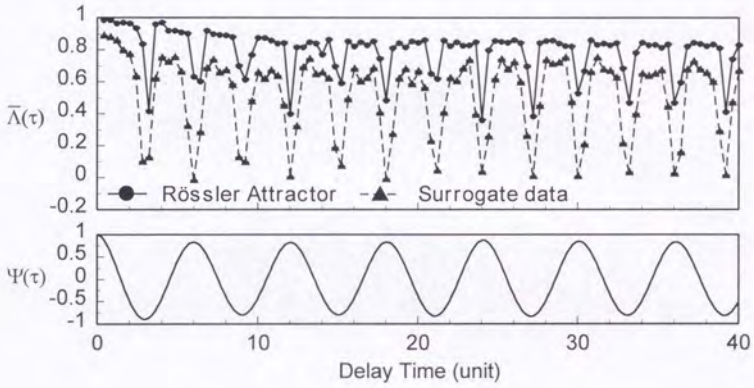

Fig. 17 Results of Kaplan-Glass algorithm from the Rössler attractor and the surrogate data. The weighted mean of the average directional vectors of all the hyper cubes passed through by the trajectory $\overline{\Lambda}$, and the autocorrelation function Ψ are plotted against the delay time τ. The embedding dimension is three, and the gridding is 16^3. $\overline{\Lambda} \equiv 1$ for completely deterministic systems, and $\overline{\Lambda} \equiv 0$ for completely random dynamics like Gaussian white noise.

Fig. 18, 19, and 20 show $\overline{\Lambda}$ and the autocorrelation function Ψ plotted against the delay time τ. Both $\overline{\Lambda}$'s from the subject data and the simulated data were larger than zero because of deterministic characteristics such as the periodicity of both data. The $\overline{\Lambda}$'s reached minima whenever Ψ was at an extremum, because the embedded time series has a narrow ellipsoid shape in such cases, and both the ascending and descending limbs of the trajectory may pass through the same box. If $\overline{\Lambda}$ from the subject data is significantly larger than that from the simulated data, it proves the presence of a deterministic process which creates breath-to-breath variability. However, there were no significant differences in $\overline{\Lambda}$'s between the subject and simulated data. Results from the other five subjects were essentially the same as those from subject #5.

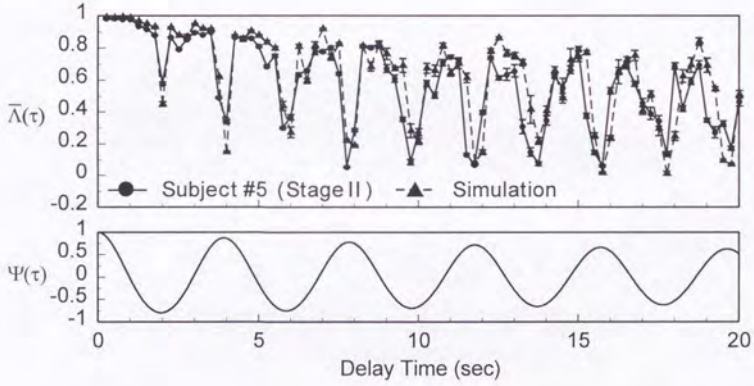

Fig. 18 Results of Kaplan-Glass algorithm from the data of subject #5 at stage II sleep. The embedding dimension is six, and the gridding is 16^6.

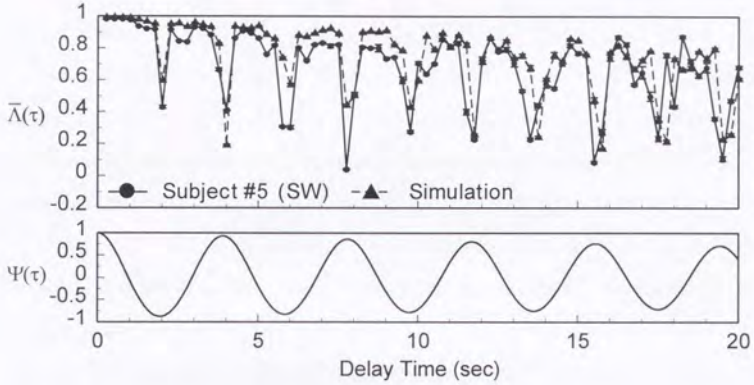

Fig. 19 Results of Kaplan-Glass algorithm from the data of subject #5 at SW sleep. The embedding dimension is six, and the gridding is 16^6.

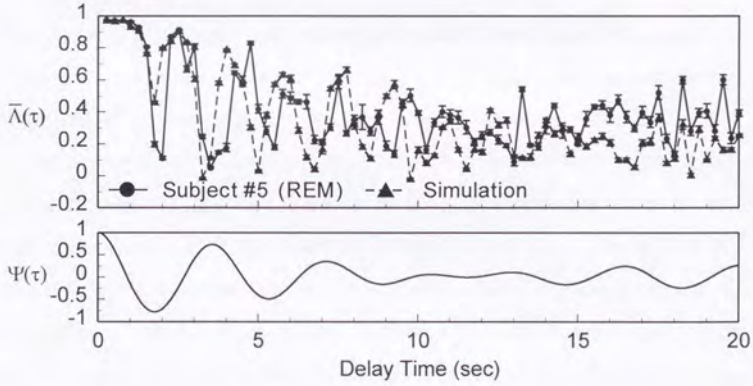

Fig. 20 Results of Kaplan-Glass algorithm from the data of subject #5 at REM sleep. The embedding dimension is six, and the gridding is 16^6.

IV. DISCUSSION

Respiratory phase and depth fluctuate even when an individual is in a steady state and external perturbations are minimal. It is reasonable to hypothesize that these fluctuations are due to chaotic or quasiperiodic dynamics of the respiratory control system rather than random processes, since:

(1) It is likely that timing and depth of each breath are controlled to the optimal values by the respiratory control system including the central rhythm generator and several feedback loops[47].

(2) The respiratory control system consists of multiple feedback loops with time delays. This structure is one of the common system structures which show chaotic behavior[48].

(3) There are quite a few studies arguing that respiratory parameters of several successive breaths are significantly correlated[5-7], or that respiratory rhythm is a superimposition of several different oscillations[1-3].

To date, there have been three studies published on this issue, using the techniques of nonlinear dynamics. Donaldson[20] argued that respiration in resting humans was chaotic, based on the positive Lyapunov exponent calculated using the WSSV algorithm[24]. However, his graphs showed that the estimate of the Lyapunov exponent was variable according to such parameters as the evolution time and the delay time, which strongly suggested that it was a spurious positive value similar to the values we obtained from both our experimental and simulated data sets. Thus, we feel that this does not indicate chaotic behavior. Sammon *et al.*[19] studied rats, and concluded that respiration in rats with intact vagi was chaotic, while respiration in vagotomized rats was periodic. They showed "V" shaped return maps of lung volume as evidence of chaos, but the estimate of the correlation dimension in some of their vagi-intact rats seemed to increase with each increment of the embedding dimension without approaching an asymptote. DeGoede *et al.*[21] concluded that the flow signal obtained from cats was not chaotic but a noisy limit cycle because the correlation dimension did not approach an asymptote but continued to increase with the increment of the embedding

dimension. Hence, it is still controversial whether the fluctuations of respiratory parameters originate from deterministic dynamics or not.

As one can easily notice from the raw data (Fig. 3), respiration has a strong periodicity with a mean orbital period (in our subjects) of about four seconds, but if one examines the breath-to-breath variability, it appears to be nonperiodic. This kind of behavior may represent chaos, quasiperiodicity, or noisy periodicity. Thus, the purpose of this study was to determine which of these three categories of dynamics best describes respiration. It is sometimes very difficult to distinguish chaos from quasiperiodicity with the existence of intrinsic or measurement noise. Therefore, we produced a noisy limit cycle as the null hypothesis which could not be distinguished from the experimental data by eye, and we tried to find significant differences between the data and the null hypothesis as evidence of determinism, *i. e.* chaos or quasiperiodicity, using several algorithms of nonlinear dynamics.

As described in the Results section, no significant differences between the subject data and the simulated data were found by using any of the algorithms employed in the study. This fact leads us to one of the following four conclusions:

(1) The dynamics of respiration cannot be determined because it is obscured by measurement noise.

(2) Breath-to-breath variability of respiratory parameters is due to random fluctuations of the respiratory controlling system.

(3) The variability is due to deterministic dynamics, but the dimension of the attractor is so high that the algorithms fail to detect determinism in the data sets, which are of limited size.

(4) The dynamics of respiration cannot be determined because it is not steady even within the same sleep stage.

Before discussing the other possibilities, it is important to address the issue of measurement noise. To assess the permissible level of noise is difficult, because it depends on the characteristics of the noise, the algorithm in use, the size of the data set, and the dimension of the attractor. Furthermore, although there are some studies on the effects of

additive white noise in the calculations of the dimension and the Lyapunov exponents[49-51], the noise in our data seems to be correlated noise due to characteristics of the RIP rather than uncorrelated white noise or high-frequency noise such as the noise from an electric power supply.

The RIP is a device which measures lung volume changes by assessing the changes in cross-sectional area of the rib cage and the abdominal cavity. That is to say $V = (c_1 S_{RC} + S_{Abd})c_2$, where V is the volume change of the lungs, S_{RC} and S_{Abd} denote the signals from the bands wrapped around the rib cage and the abdomen respectively, c_1 is the coefficient which represents the ratio of the signals from the rib-cage and abdominal bands for the same change of lung volume, and c_2 is the coefficient to convert voltage to volume measurements. The coefficient c_2 is not important in our analysis, because the absolute value of the lung volume does not affect the results of the calculations. Thus, the factors which may produce noise are:

(a) the quantization effect due to A/D conversion,

(b) inaccuracy of the coefficient c_1, which is sensitive to the posture of the subject,

(c) disagreement of the RIP signals with lung volume owing to measuring three-dimensional quantity (volume) of each compartment by only one band,

(d) instability of the device, *i.e.* zero-drift and the fluctuations in sensitivity.

The quantization effect was smaller than 0.1% of the maximal tidal volume, because the precision of the A/D converter was 12 bits, and the intensity of the signal was at least a quarter of the full range. As well, the instability of the device was insignificant; the RIP was set to the automatic zero mode, and the fluctuations in sensitivity were found to be negligible by a supplementary experiment using a balloon (as a model of the lungs) ventilated by a mechanical ventilator which kept the tidal volume constant. Fig. 21 shows the comparison of the measurements made by two devices, the RIP and the spirometer. Tidal volume and total respiratory time measured by the RIP corresponded very well with those values measured simultaneously by a spirometer. Thus, the RIP is quite accurate when properly calibrated.

However, the question of whether or not the noise level in the data is acceptable still remains unanswered, because the properties of the attractor are unknown.

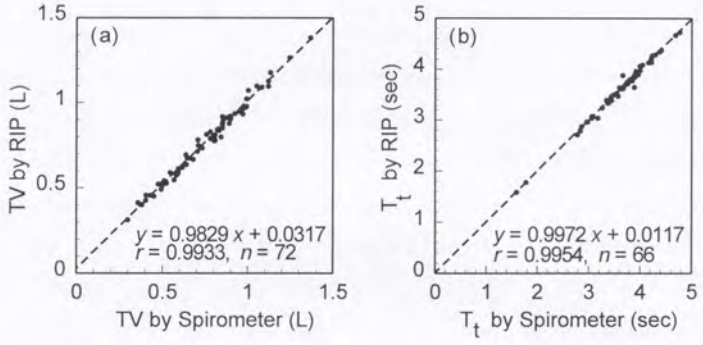

Fig. 21 Comparison of two apparatuses to measure lung volume. (a) Tidal volume and (b) Total respiratory time measured by a spirometer and a respiratory inductive plethysmograph (RIP).

Unless we can obtain larger data sets, there is no way of eliminating (2) as a possible conclusion. With regard to (3), our perception is that the dynamics of the respiratory controlling system does not change so frequently at least in stage I, II, and SW sleep. In order to examine if the results of the calculations are different from one subset to another of the same data set, we divided the data in each sleep stage into two to eight parts and calculated the correlation dimension of those subsets. No significant differences were found in the results among these data sets. The study of Pack *et al.*[52] supports our assumption, although it was a study on elderly subjects. They found clear relationships between the oscillations in ventilation and the electroencephalogram in stage I and II sleep, which means that we can assume the stability of the dynamics of respiration while the pattern of the electroencephalogram is in a steady state.

In conclusion, we could not find any clear evidence that low-dimensional determinism is the source of breath-to-breath variability of respiratory patterns in normal subjects. This suggests that the variability results from intrinsic random fluctuations or high-dimensional deterministic dynamics of the respiratory controlling system, although we cannot completely abandon the possibility of low-dimensional deterministic dynamics being obscured by measurement noise. This conclusion does not agree with our hypothesis. One conceivable explanation for this disagreement is that we used too short a study interval, *i.e.* one breath. In other words, the control of respiration works rather slowly, and it is fuzzy at the breath-to-breath level. Respiration is by no means a completely random process, since the blood gas level is maintained in a very narrow range. However, the control of the blood gasses caused by the feedback loop involving chemoreceptors has a longer time course than the duration of each breath, and this feedback loop does not seem to play an important role in generating the breath-to-breath fluctuation[5]. It would be likely that the control of timing and depth of each breath has some instability. This fuzzy control of respiration can be compared to driving a car. The locus of the car fluctuates randomly within the lane, although the course of the car is strictly controlled toward the destination. It is possible that if we extended our study to fluctuations of a time constant longer than the period of one breath the conclusions may have been different.

Finally, we emphasize that one should be aware of the limitations of the algorithms when attempting to detect chaos in biological phenomena, and that it is essential to choose an adequate system of nonchaotic dynamics as the null hypothesis to interpret the results correctly.

ACKNOWLEDGMENTS

The author is deeply grateful to Arthur S. Slutsky for his kind supervision, Kezheng Gan and Victor Hoffstein for their great collaboration in performing the experiments and the data analysis, Leon Glass and Daniel T. Kaplan for the fruitful discussion on this issue and their kind encouragement, and Kazuyuki Aihara for his useful suggestions concerning the algorithms. The author also thanks Susan Mateika for her technical help at the sleep laboratory. This study was partly supported by the Heart and Stroke Foundation of Ontario, Canada.

REFERENCES

1. L. Goodman, "Oscillatory behavior of ventilation in resting man," IEEE Trans. Biomed. Eng. BME-11, 82-93 (1964)

2. L. Goodman, D. M. Alexander, and D. G. Fleming, "Oscillatory behavior of respiratory gas exchange in resting man," IEEE Trans. Biomed. Eng. BME-13, 57-64 (1966)

3. C. Lenfant, "Time-dependent variations of pulmonary gas exchange in normal man at rest," J. Appl. Physiol. 22, 675-684 (1967)

4. M. P. Hlastala, B. Wranne, and C. J. Lenfant, "Cyclical variations in FRC and other respiratory variables in resting man," J. Appl. Physiol. 34, 670-676 (1973)

5. G. Benchetrit and F. Bertrand, "A short-term memory in the respiratory centres: statistical analysis," Respir. Physiol. 23, 147-158 (1975)

6. M. Modarreszadeh, E. N. Bruce, and B. Gothe, "Non random variability in respiratory cycle parameters of humans during stage 2 sleep," J. Appl. Physiol. 69, 630-639 (1990)

7. M. F. Khatib, Y. Oku, and E. N. Bruce, "Contribution of chemical feedback loops to Breath-to-breath variability of tidal volume, "Respir. Physiol. 83, 115-127 (1991)

8. P. J. Brusil, T. B. Waggener, R. E. Kronauer, and P. Gulesian, Jr., "Methods for identifying respiratory oscillations disclose altitude effects," J. Appl. Physiol. 48, 545-556 (1980)

9. I. P. Priban, "An analysis of some short-term patterns of breathing in man at rest," J. Physiol. London 166, 425-434 (1963)

10. D. P. G. Bolton and J. Marsh, "Analysis and interpretation of turning points and run length in breath-by-breath ventilatory variables," J. Physiol. London 351, 451-459 (1984)

11. P. Dejours, R. Puccinelli, J. Armand and M. Dicharry, "Breath-to-breath variations of pulmonary gas exchange in resting man," Respir. Physiol. 1, 265-280 (1966)

12. H. Degn, A. V. Holden, and L. F. Olsen (Eds.), *Chaos in Biological Systems* (Plenum Press, New York, 1987)

13. M. C. Mackey and L. Glass, "Oscillation and chaos in physiological control systems," Science 197, 287-289 (1977)

14. T. Pham Dinh, J. Demongeot, P. Baconnier, and G. Benchetrit, "Simulation of a biological oscillator: the respiratory system," J. Theor. Biol. 103, 113-132 (1983)

15. G. A. Petrillo, L. Glass, and T. Trippenbach, "Phase locking of the respiratory rhythm in cats to a mechanical ventilator," Can. J. Physiol. Pharmacol. 61, 599-607 (1983)

16. C. Graves, L. Glass, D. Laporta, R. Meloche, and A. Grassino, "Respiratory phase locking during mechanical ventilation in anesthetized human subjects," Am. J. Physiol. 250, R902-R909 (1986)

17. J. Lewis, M. Bachoo, C. Polosa, and L. Glass, "The effects of superior laryngeal nerve stimulation on the respiratory rhythm: phase-resetting and aftereffects," Brain Research 517, 44-50 (1989)

18. S. M. Botros and E. N. Bruce, "Neural network implementation of a three-phase model of respiratory rhythm generation," Biol. Cybern. 63, 143-153 (1990)

19. M. P. Sammon and E. N. Bruce, "Vagal afferent activity increases dynamical dimension of respiration in rats," J. Appl. Physiol. 70, 1748-1762 (1991)

20. G. C. Donaldson, "The chaotic behaviour of resting human respiration," Respir. Physiol. 88, 313-321 (1992)

21. J. DeGoede, E. Olofsen, and A. Berkenbosch, presented at the workshop on "Models of complex respiratory dynamics in sleep and wakefulness," Anaheim, Ca., 1991 (unpublished)

22. P. Grassberger and I. Procaccia, "Measuring the strangeness of strange attractors," Physica 9D, 189-208 (1983)

23. P. Grassberger and I. Procaccia, "Characterization of strange attractors," Phys. Rev. Lett. 50, 346-349 (1983)

24. A. Wolf, J. B. Swift, H. L. Swinney, and J. A. Vastano, "Determining Lyapunov exponents from a time series," Physica 16D, 285-317 (1985)

25. G. Sugihara and R. M. May, "Nonlinear forecasting as a way of distinguishing chaos from measurement error in time series," Nature 344, 734-741 (1990)

26. D. T. Kaplan and L. Glass, "Direct test for determinism in a time series," Phys. Rev. Lett. 68, 427-430 (1992)

27. D. T. Kaplan and L. Glass, "Coarse-grained embeddings of time series: random walks, Gaussian random processes, and deterministic chaos," Physica 64D, 431-454 (1993)

28. R. Gilbert, J. H. Auchincloss, Jr., J. Brodsky, and W. Boden, "Changes in tidal volume, frequency, and ventilation induced by their measurement," J. Appl. Physiol. 33, 252-254 (1972)

29. J. Askanazi, P. A. Silverberg, R. J. Foster, A. I. Hyman, J. Milic-Emili, and J. M. Kinney, "Effects of respiratory apparatus on breathing pattern," J. Appl. Physiol. 48, 577-580 (1980)

30. W. Perez and M. J. Tobin, "Separation of factors responsible for change in breathing pattern induced by instrumentation," J. Appl. Physiol. 59, 1515-1520 (1985)

31. M. J. Tobin, M. J. Mador, S. M. Guenther, R. F. Lodato, and M. A. Sackner, "Variability of resting respiratory drive and timing in healthy subjects," J. Appl. Physiol. 65, 309-317 (1988)

32. T. S. Chada, H. Watson, S. Birch, G. A. Jenouri, A. W. Schneider, M. A. Cohn, and M. A. Sackner, "Validation of respiratory inductive plethysmography using different calibration procedures," Am. Rev. Respir. Dis. 125, 644-649 (1982)

33. A. Rechtschaffen and A. Kales, *A Manual of Standardized Terminology, Techniques and Scoring System for Sleep States of Human Subjects*, National Institutes of Health Publication no. 204, Washington, D. C. (1968)

34. A. Savitzky and M. J. E. Golay, "Smoothing and differentiation of data by simplified least square procedures," Anal. Chem. 36, 1627-1639 (1964)

35. F. Takens, "Detecting strange attractors in turbulence," in *Lecture Notes in Mathematics 898*, edited by A. Dold and B. Eckmann (Springer-Verlag, Berlin, 1981), pp. 366-381

36. G. Mayer-Kress, "Application of dimension algorithms to experimental chaos," in *Directions in Chaos 1*, edited by B-L. Hao (World Scientific, Singapore, 1987), pp. 122-147

37. A. M. Albano, A. I. Mees, G. C. de Guzman, and P. E. Rapp, "Data requirements for reliable estimation of correlation dimensions," in *Chaos in Biological Systems*, edited by H. Degn, A. V. Holden, and L. F. Olsen (Plenum Press, New York, 1987), pp. 207-220

38. J. Theiler, "Spurious dimension from correlation algorithms applied to limited time-series data," Phys. Rev. A 34, 2427-2432 (1986)

39. G. W. Frank, T. Lookman, M. A. H. Nerenberg, C. Essex, J. Lemieux, and W. Blume, "Chaotic time series analyses of epileptic seizures," Physica 46D, 427-438 (1990)

40. O. E. Rössler, "An equation for continuous chaos," Phys. Lett. A. 57, 397-398 (1976)

41. E. N. Lorenz, "Deterministic nonperiodic flow," J. Atmos. Sci. 20, 130-141 (1963)

42. J. D. Farmer and J. J. Sidorowich, "Predicting chaotic time series," Phys. Rev. Lett. 24, 845-848 (1987)

43. M. Casdagli, "Nonlinear prediction of chaotic time series," Physica 35D, 335-356 (1989)

44. A. I. Mees, "Modelling complex systems," in *Dynamics of Complex Interconnected Biological Systems*, edited by T. L. Vincent, A. I. Mees, L. S. Jennings (Birkhäuser, Boston, 1990), pp. 104-124

45. J. Jiménez, J. A. Moreno, and G. J. Ruggeri, "Forecasting on chaotic time series: a local optimal linear-reconstruction method," Phys. Rev. A. 45, 3553-3558 (1991)

46. R. H. Harding and J. Ross, "The effect of different types of noise on some methods of distinguishing chaos from periodic oscillations," J. Chim. Phys. 84, 1305-1313 (1987)

47. C. von Euler, "Neural organization and rhythm generation," in *The Lung: Scientific Foundations*, edited by R. G. Crystal, J. B. West, et al. (Raven Press, Ltd., New York, 1991), pp. 1307-1318

48. L. Glass and C. P. Malta, "Chaos in multi-looped negative feedback systems," J. Theor. Biol. 145, 217-223 (1990)

49. T. Geisel, "Chaos and noise," in *Chaos in Astrophysics*, edited by J. R. Buchler, J. M. Perdang, and E. A. Spiegel (D. Reidel Publishing, Dordrecht, 1985), pp. 165-183

50. W. M. Schaffer, S. Ellner, and M. Kot, "Effects of noise on some dynamical models in ecology," J. Math. Biol. 24, 479-523 (1986)

51. M. Möller, W. Lange, F. Mitschke, N. B. Abraham, and U. Hübner, "Errors from digitizing and noise in estimating attractor dimensions," Phys. Lett. A 138, 176-182 (1989)

52. A. I. Pack, M. F. Cola, A. Goldszmidt, M. D. Ogilvie, and A. Gottschalk, "Correlation between oscillations in ventilation and frequency content of the electroencephalogram," J. Appl. Physiol. 72, 985-992 (1992)

Appendix: Glossary of terms in nonlinear dynamics

Attractor: A set of trajectories in phase space toward which a time history of a system approaches after transient responses die out. Fixed points, limit cycles (closed circuits), toroidal surfaces, and fractals are attractors of equilibrium, periodicity, quasiperiodicity, and chaos respectively.

Autocorrelation: Denotes a measure of how closely a time series resembles a time-delayed image of itself. Periodic time series are highly autocorrelated whereas random series are not.

Chaos: A type of motion of a deterministic system that is nonperiodic and sensitive to changes in initial conditions. The trajectories starting from slightly different initial conditions diverge exponentially, so it is impossible to predict the state of the system in the distant future. The attractor of a chaotic system usually has a fractal structure.

Deterministic: A system is deterministic if it is described by known equations and does not contain random component. The evolution of a deterministic system is completely determined by its current state and past history.

Embedding: A technique of reconstructing a geometrical figure that is topologically equivalent (homeomorphism) to the attractor of a system from a time series of only one variable, using time delay coordinates.

Fractal: Denotes a geometric property of a set of points which have the quality of self-similarity at differential length scales.

Fractal dimension: A quantitative property of a set of points which measures the way the points fill a given area of space. There are infinite number of generalized fractal dimensions, among which the correlation dimension is the easiest to calculate.

Limit cycle: Denotes, in the engineering literature, a periodic motion that arises from an autonomous system. In the dynamical systems literature, it also includes forced periodic motions. The attractor of a limit cycle is a closed curve. The fractal dimension and the Lyapunov exponent is one and zero respectively.

Lyapunov exponent: A positive Lyapunov exponent means the exponential divergence of nearby trajectories, i. e. sensitive dependence of the system on initial conditions.

Noise: Usually denotes the small random background disturbances of any origin, *e. g.* mechanical, thermal, or electrical.

Noisy limit cycle: A limit cycle (periodic motion) contaminated with a noise of any kind. If the noise is not an uncorrelated (white) noise but a correlated (coloured) noise, it may be difficult to distinguish a noisy limit cycle from a deterministic dynamics *i. e.* chaos or quasiperiodicity.

Phase space: An n-dimensional space of which coordinates denote the state variables of a dynamical system. The state of the system at a certain time is equivalent to a point in the phase space.

Quasiperiodicity: Denotes a vibration motion consisting of two or more incommensurate frequencies. The fractal dimension is an integer number that is equal to the number of frequencies. The maximal Lyapunov exponent is zero.

Return map: A graphic technique that represents the relation between a point and any subsequent point in a time series.

Strange attractor: Refers to the attractor on which chaotic orbits move. Strange attractors have fractal structure.

Trajectory: Denotes the representation of the behaviour of a system in phase space over a short period of time.

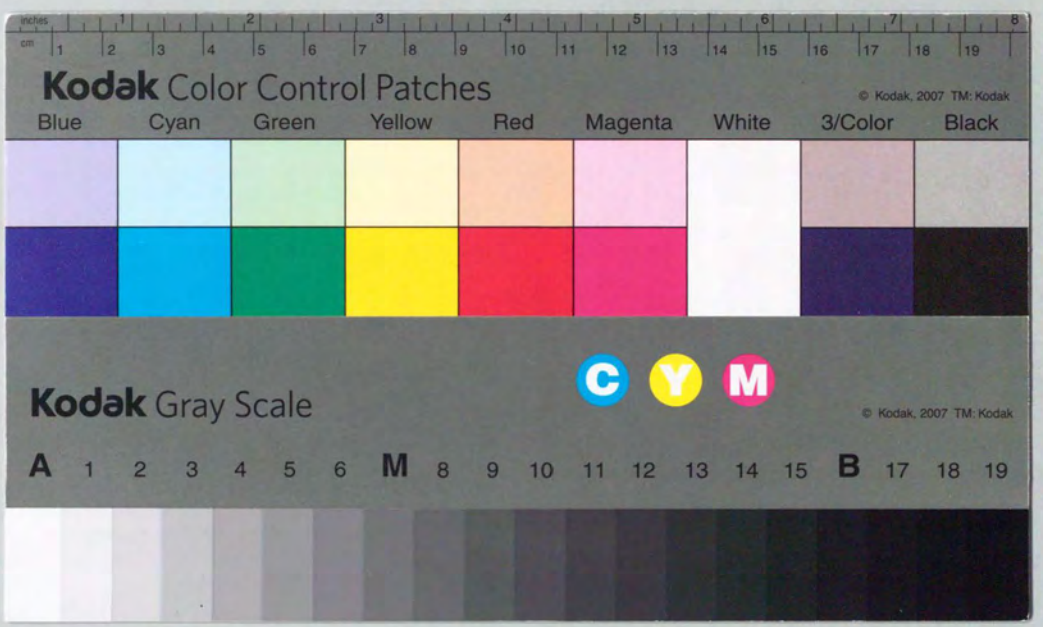
inches
cm
1 2 3 4 5 6 7 8
1 2 3 4 5 6 7 8 9 10 11 12 13 14 15 16 17 18 19
Kodak Color Control Patches
© Kodak, 2007 TM: Kodak
Blue
Cyan
Green
Yellow
Red
Magenta
White
3/Color
Black
Kodak Gray Scale
C
Y
M
© Kodak, 2007 TM: Kodak
A 1 2 3 4 5 6 M 8 9 10 11 12 13 14 15 B 17 18 19